

Three-Dimensional Imaging by Self-Reference Single-Channel Digital Incoherent Holography

Joseph Rosen and Roy Kelner

Abstract—Digital holography offers a reliable and fast method to image a three-dimensional (3-D) scene from a single perspective. This paper reviews recent developments of self-reference single-channel incoherent hologram recorders. Hologram recorders in which both interfering beams, commonly referred to as the signal and the reference beams, originate from the same observed objects are considered as self-reference systems. Moreover, the hologram recorders reviewed herein are configured in a setup of a single-channel interferometer. This unique configuration is achieved through the use of one or more spatial light modulators (SLMs).

Index Terms—Confocal microscopy, digital holography, spatial light modulators (SLMs), three-dimensional (3-D) image acquisition.

I. INTRODUCTION

DIGITAL holography has several advantages for many imaging applications. The most recognized advantage of digital holography is its ability to image a three-dimensional (3-D) scene with no more than three camera shots [1]. Additionally, hologram recorders of certain types are capable of imaging phase objects [2], [3]. Different types of hologram recorders have been proved to have superior imaging resolution over equivalent ordinary imagers [4], [5]. Digital holography also enables the implementation of super-resolution techniques such as synthetic aperture [6], [7]. Moreover, using holograms, it is possible to image objects covered by scattering medium [8], [9], or by absorbing obstacles [10], [11]. Additionally, digital holography can be used for certain tasks of image processing, such as edge enhancement [12], [13]. Finally, some holographic imagers have been proved quite efficient for sectioning a general 3-D scene [14], [15]. Because of these advantages, digital holography has become an important tool for optical imaging in general and for optical microscopy in particular.

In the present review, the research in which we have been involved in the recent years is summarized. Two operation

Manuscript received March 31, 2015; revised June 11, 2015; accepted July 03, 2015. Date of publication July 30, 2015; date of current version August 04, 2016. This work was supported in part by the National Institutes of Health (NIH) under Grant U54GM105814, in part by the Israel Ministry of Science and Technology (MOST), and in part by the Israel Science Foundation (ISF) (439/12). A short version of this paper has been published as a conference paper in [78]. The conference paper [78] does not include the discussions about the resolution properties of the systems and their optical path difference problem (II-C and II-D herein). On the other hand and unlike this paper, [78] surveys also the works first published in [17] and [20]. Paper no. TII-15-0513.

The authors are with the Department of Electrical and Computer Engineering, Ben-Gurion University of the Negev, Beer-Sheva 8410501, Israel (e-mail: rosen@ee.bgu.ac.il; kelnerr@post.bgu.ac.il).

Color versions of one or more of the figures in this paper are available online at <http://ieeexplore.ieee.org>.

Digital Object Identifier 10.1109/TII.2015.2462803

principles are common to the hologram recorders discussed herein. First, as indicated by the title, the various holograms are recorded in a self-reference setup, which means that the interfering beams originate from the same observed object. As is shown below, this property of the systems enables hologram recording of objects that are illuminated by spatially incoherent sources. However, the self-reference arrangement is efficient also for temporally [16], [17] or spatially [18], [19] coherent light sources, since it saves the need to split the light source into two separated beams, one for the reference beam and the other for the signal beam. The second principle is that the hologram recorders are configured as single-channel interferometers. The configuration in a single channel makes this type of systems more stable, robust, and easier to align than the dual channel interferometers. Nevertheless, the hologram is still recorded as interference between pairs of beams inside the single channel. The beam splitting inside the single optical channel is achieved due to the use of a phase-only spatial light modulator (SLM), which is a crucial element in all of the systems described in this paper. The research described herein has been focused in the field of incoherent digital holography. Here, the term incoherence actually means spatial incoherence, in the sense that each infinitesimal object point (i.e., point source) is statistically uncorrelated with any other object point. As for the temporal coherence, the spatial incoherent systems described in this review use narrowband light. Therefore, if the chromatic filters are an integral part of the systems, then these holographic recorders can be considered also as temporally incoherent, operating with white light. Otherwise, they may be classified as partially temporally coherent systems.

One of the most explored methods of incoherent holography in recent years is the Fresnel incoherent correlation holography (FINCH). Section II is devoted to FINCH, with its various versions. Section III deals with another incoherent recorder termed Fourier incoherent single-channel holography (FISCH). Our group recently started to explore the use of self-reference, SLM aided, hologram recorders in the regime of coherent digital holography [17], [20]. Due to space limitations, this type of hologram recorders is not reviewed herein.

II. FRESNEL INCOHERENT CORRELATION HOLOGRAPHY

A. Early Versions

In the early years of the present millennium, the field of incoherent digital holography was mainly dominated by two acquisition methods of incoherent holograms. One method is known under the name optical scanning holography (OSH)

[21], while the other method is termed multiple view projection (MVP) holography [22]. Both of these methods are relatively slow, since a scanning over the observed object is needed in OSH, and capturing of multiple images is required in MVP systems. Therefore, faster hologram recorders suitable for incoherently illuminated scenes seemed necessary, at that time. A faster nonscanning alternative to OSH and MVP can be self-reference interferometric methods [23]–[30], which use the property that an incoherent light source is assembled from multiple statistically independent points, each of which can induce an interference pattern only with light coming from the point and from its copied image, or from two different images of the same point source. In this kind of interferometers, the light wave from each object point is split into two mutually coherent beams, each of which is optically processed differently; later, both beams are interfered on the hologram plane. The resulting hologram contains the information on the 2-D [23], [25], [27], [29] or 3-D [24], [26], [28], [30] location of each object point. FINCH also belongs to this group of self-reference hologram recorders, but, as described next, is based on several new principles.

Since its introduction in 2007 [31], FINCH has earned the attention of several research groups around the world [8], [9], [12], [32]–[48]. This may be attributed to many contributing factors, including the simple working principle of FINCH, its common-path single-channel design and, most importantly, its ability to record the complete 3-D information of spatially incoherent objects. Among the works which have been constructed on the basis of FINCH, in recent years, are the FINCH-based fluorescence microscope (FINCHSCOPE) [49] and its most current, highly efficient version based on a liquid crystal gradient index lens [50], making the FINCHSCOPE highly appealing for biological applications. A noteworthy FINCH-related technique is the self-interference incoherent digital holography (SIDH), in which the SLM-aided single channel of FINCH is replaced by a modified Michelson interferometer with two mirrors of different spherical curvatures [51]–[53]. Another interesting design in this context is a FINCH-like system with a wide field-of-view that is achieved using an optical relay system placed between two main components of FINCH: 1) the objective lens; and 2) the SLM [54]. Other examples of FINCH-based imagers include the synthetic aperture with Fresnel elements (SAFE) systems [55]–[57]. SAFE is an incoherent holographic imaging system in which a super-resolving synthetic aperture hologram is formed as a mosaic of several holograms captured from different points of view by a regular FINCH system, which has a limited physical aperture. It is beyond the scope of this review to extensively cover every modification and application of FINCH. Hence, only several structural developments of FINCH are surveyed herein.

Essentially, FINCH is also a self-reference interferometric method, but the splitting of the light beam is accomplished within a single optical channel. In other words, FINCH is implemented by a single channel, on-axis, spatially incoherent interferometer. Therefore, FINCH is more stable, robust, easier to align, and can handle light in wider bandwidth in comparison to other classical dual channel interferometric methods. All these benefits are achieved using an SLM within the FINCH

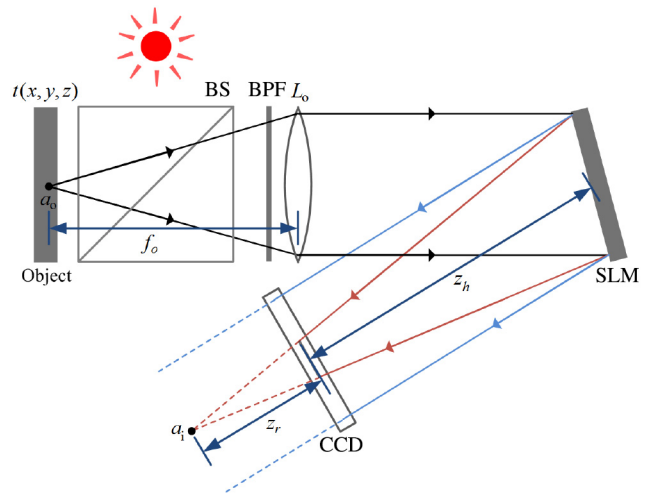


Fig. 1. Schematic of the first FINCH recorder: BS, beam splitter; BPF, band-pass filter; SLM, spatial light modulator; CCD, charge-coupled device.

apparatus. The role of the SLM will become clearer following the next description of FINCH.

The first FINCH setup [31] is shown in Fig. 1. In this holographic recorder, spatially incoherent light is emitted from, or scattered by, a 3-D object. It is then collected into the system by the objective lens L_o and modulated by an SLM. The SLM serves both as a beam-splitter and as a diffractive lens. In this manner, a single-channel incoherent interferometer is formed. In the interferometer, each spherical beam that originates from a single object point is split into two spherical beams of different curvatures. A Fresnel hologram of a point source is obtained when the interference pattern of the two spherical beams is recorded by a digital camera. The need to create two different spherical beams is fulfilled by generating a diffractive lens using only a half of all SLM pixels. The pixels of one lens are randomly selected and uniformly distributed. The remaining pixels are modulated with a constant phase [4], [31], [49], [58], or are used to create a different diffractive lens than the first one [59]. In any case, once a wave from a point source reaches the SLM, two spherical waves are reflected from the SLM and interfere on the digital camera plane. The spatial incoherence of the object assures that the final recorded FINCH hologram is a summation over the intensities of all point source interference patterns. This summation forms the Fresnel hologram of the observed 3-D object. The recorded object can then be reconstructed from the hologram through a digital Fresnel back-propagation to a specific reconstruction distance.

FINCH captures Fresnel holograms of the scene. By definition, a Fresnel hologram contains a transparency function of the convolution between the object and a quadratic phase function [60]. However, the case in FINCH is a bit more complicated. For a general 3-D object, incoherently illuminated by a narrowband light source, the intensity of the recorded FINCH hologram is a convolution between the object intensity function and the point spread function (PSF) of the system. The PSF of the recorder, for the case of a point source located on the front focal plane of lens L_o of Fig. 1, at an arbitrary lateral location $\vec{r}_s = (x_s, y_s)$, is a hologram. This hologram is

obtained by the interference between a spherical wave converging to the image point a_i , located at a distance z_r from the charge-coupled device (CCD) plane at the lateral point $[-(z_h + z_r)x_s/f_o, -(z_h + z_r)y_s/f_o]$, and a slanted plane wave with declination angles $(\theta_x, \theta_y) = [\arctan(x_s/f_o), \arctan(y_s/f_o)]$, where z_h is the gap between the SLM and the CCD and f_o is the focal length of the lens L_o . Hence, for a point of intensity $I_s(x_s, y_s)$, the hologram is

$$\begin{aligned}
 h(x, y) &= I_s(\bar{r}_s) \\
 &\left| \exp \left\{ \frac{-j\pi}{\lambda z_r} \left[\left(x + \frac{(z_h + z_r)x_s}{f_o} \right)^2 + \left(y + \frac{(z_h + z_r)y_s}{f_o} \right)^2 \right] \right\} \right. \\
 &+ \exp \left(-j \frac{2\pi(x_s x + y_s y)}{\lambda f_o} \right) \left. \right|^2 = I_s(\bar{r}_s) \left(2 \right. \\
 &+ \exp \left\{ \frac{j\pi}{\lambda z_r} \left[\left(x + \frac{z_h x_s}{f_o} \right)^2 + \left(y + \frac{z_h y_s}{f_o} \right)^2 \right] + j\phi(\bar{r}_s) \right\} \\
 &+ \left. \exp \left\{ \frac{-j\pi}{\lambda z_r} \left[\left(x + \frac{z_h x_s}{f_o} \right)^2 + \left(y + \frac{z_h y_s}{f_o} \right)^2 \right] - j\phi(\bar{r}_s) \right\} \right)
 \end{aligned} \tag{1}$$

where λ is the average wavelength and $\phi(\bar{r}_s)$ is a phase constant.

The overall hologram of the object, for the above case, is an integral over all the object points as follows:

$$\begin{aligned}
 H(x, y) &= C + 2 \iint I_s(\bar{r}_s) \\
 &\times \cos \left\{ \frac{\pi}{\lambda z_r} \left[\left(x + \frac{z_h x_s}{f_o} \right)^2 + \left(y + \frac{z_h y_s}{f_o} \right)^2 \right] \right. \\
 &\left. + \phi(\bar{r}_s) \right\} dx_s dy_s
 \end{aligned} \tag{2}$$

where C is a constant. Equation (2) indicates that besides a relatively high constant term, the transparency function of the hologram contains two terms of convolution, one between the object and a quadratic z -dependent phase function, and another between the object and the complex conjugate of the same quadratic phase function. Reconstructing a hologram with these three terms does not enable proper extraction of the 3-D image of the object, because of mutual disturbance between the terms. This difficulty is well known in the literature as the twin-image problem [60]. In order to remain with only a single convolution term out of the three terms, a phase-shifting procedure is performed with the reordered holograms [31]. Three holograms of the same object are recorded, each with a different phase constant, adjacent only to one of the diffractive lenses that are displayed on the SLM. Thus, a third task is added to the SLM, which serves as a phase-shifter, a beam-splitter, and a diffractive lens. The final hologram is a linear combination of the three holograms; it contains only the desired convolution term between the object function and a single z -dependent quadratic phase function. This final phase-shifted hologram can be digitally reconstructed using a computer. A Fresnel back-propagation calculation properly reveals the 3-D properties of the object, without noise from other interference terms.

This early version of FINCH was demonstrated in various studies and under different conditions. First, it was demonstrated with reflecting, white-light illuminated objects [31]. Later, FINCH holograms of fluorescence objects of various colors were successfully recorded [58]. Shortly after, a complete FINCH-based holographic fluorescence microscope was proposed and demonstrated [49]. However, the performances of these early versions of FINCH were not optimal. The above-described method of multiplexing two diffractive lenses on the SLM induced a lot of noise. Many parameters in the system were arbitrarily chosen, and the optical path difference (OPD) in the system, which limits the system from processing wide-bandwidth light sources, was not optimized. These problems have been successfully addressed in the more recent developments of FINCH, described in the following sections.

B. Polarization Method for Multiplexing Diffractive Elements

The configuration of FINCH as a single-channel interferometer has many advantages, mentioned above, but the need to multiplex two diffractive elements on the same SLM is a challenge as the sum of two phase functions is not a pure phase function. Therefore, such a sum cannot be displayed directly on commercially available phase-only SLMs. In the previously described multiplexing method, used in early FINCH versions, the two phase functions were displayed on different portions of the SLM. Consequently, these two optical elements were non-continuous, did not occupy the complete aperture of the system, and led to suboptimal results. A way to overcome this problem is given by the polarization method discussed next.

Fortunately, the problem of element multiplexing can be solved using the property that some commercially available phase-only SLMs, which are birefringent devices, only modulate light of a certain linear polarization orientation. This sensitivity of the SLM to a specific linear polarization makes it possible to use one component of the electric field vector, not affected by the SLM, as a wave without any modulation, and the other orthogonal component as a wave that is modulated with the desired diffractive lens. Unlike the previous spatial multiplexing method, when the polarization multiplexing method is used, both diffractive elements occupy the complete aperture of the system, and so the SLM-realized optical elements are both continuous and of better quality.

The detailed optical process of the polarization method of FINCH is described in [61]. It is summarized in the following with the help of Fig. 2. A spherical beam is emitted from a point source a_o located at a working distance from the objective lens L_o . An input polarizer P_1 is oriented at a 45° angle to the active axis of the SLM, resulting in two in-parallel imaging systems in a common-path single-channel setup. The SLM acts as a spherical lens, but only for the polarization components of the beam that are in parallel to its active axis. Polarization components of the input beam that are vertical to its active axis are not modulated; for them, the SLM is a clear aperture. Thus, each of the two in-parallel imaging systems acts with one of two orthogonal polarization components of light. The input beam from a_o is collected by the lens L_o and then converged into two

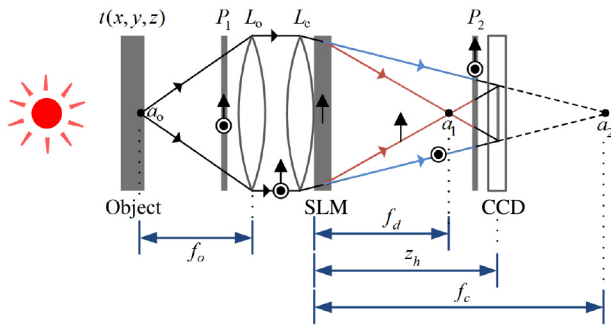


Fig. 2. Schematic of a FINCH recorder in the polarization method: P_1 and P_2 , polarizers; L_o , objective lens; L_c , converging lens; SLM, spatial light modulator; CCD, charge-coupled device. The symbols \odot , \uparrow and $\odot\uparrow$ are polarization directions perpendicular, parallel and at 45° to the plane of the page, respectively. Figure adapted from [62].

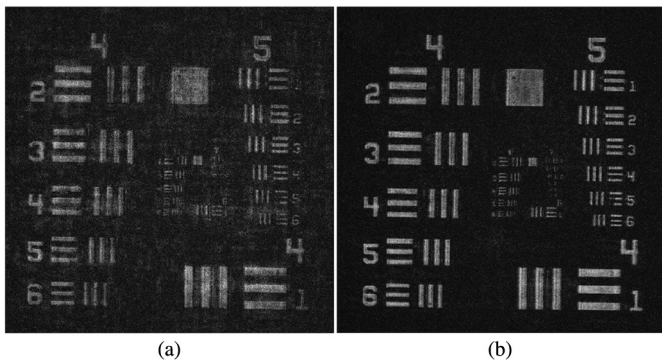


Fig. 3. Best plane of focus reconstruction from holograms of a USAF test slide using (a) spatial multiplexing with constant and quadratic-phase masks and (b) the polarization multiplexing method with input and output polarizer orientations of 45° .

image points beyond the SLM: 1) the image point a_2 , formed by the system in which the SLM does not influence the beam; and 2) the image point a_1 , formed by the system in which the SLM-displayed diffractive lens is effective. A digital camera, positioned between the two image points, captures the interference pattern of two spherical beams: 1) diverging from a_1 ; and 2) converging toward a_2 . The output polarizer P_2 enables the interference between the waves by projecting the orthogonal polarization components of the two beams onto a common orientation. Frequently, P_2 is oriented at a 45° angle to the active axis of the SLM. However, other angles can be used [61]. The hologram recording and reconstruction procedures are similar to the ones described in the previous section.

Imaging results of a United States Air Force (USAF) resolution chart with both spatial [31] and polarization [61] methods of multiplexing are compared in Fig. 3. This figure shows image reconstructions of best plane of focus obtained from holograms captured using both methods. The experimental conditions were identical, using a diffractive lens of a 280-mm focal length, with the camera positioned at a distance of 400-mm away from the SLM. In Fig. 3(a), the holograms were captured with a 50% constant phase mask and with the input and output polarizers set parallel the SLM polarization. In Fig. 3(b), the holograms were captured using the polarization method, without any constant phase mask and with

the polarizers set at 45° to the SLM polarization. The results demonstrate the superiority of the polarization method.

C. Inherent Super-Resolution

In general, recording and reconstructing a hologram is an imaging process. The most important feature of any imaging system, in general, and microscopy, in particular, is its imaging resolution. According to Abbe's law [63], in conventional imaging systems, the optical resolution is determined by the ratio between the illumination wavelength and the input numerical aperture of the system. At the beginning of the presented research [31], [58], FINCH had been considered as a conventional imaging system, obeying the same optical resolution limit. Surprisingly, several years after its invention, it was discovered that FINCH is not at all a conventional imaging system, and that under certain conditions FINCH can fundamentally resolve better than conventional imagers of similar numerical aperture [4]. The roots for this phenomenon are discussed next.

One of the most known and general laws of imaging systems is the Lagrange invariant [63]. About 4 years after the FINCH invention [31], Bouchal *et al.* were the first to propose that FINCH is exceptional, in the sense that it violates the Lagrange invariant [33]. Later, Lai *et al.* published a paper dedicated completely to this unusual violation of the Lagrange invariant [41]. Beyond the remarkable aspect of violating a fundamental imaging rule, there is also a practical aspect for this violation. As is shown in [64], there is a direct link between the Lagrange invariant and the imaging transverse and axial resolutions. The linkage between the resolutions and the Lagrange invariant is understandable if the definition of the latter is modified to the optical wave theory. Generally, infinitesimally object points are imaged by imaging systems to spots of a fixed size, where the spots on the object and the image planes are defined as the system PSF on these two planes. According to the modified Lagrange invariant, formalized in [64], for any two-point object, the spots and the gap between them are magnified equally by the imager. This law of identical magnification is natural and generally accepted when conventional imagers are regarded. However, as is shown in [64], this basic rule can be violated in any FINCH system. When this law is violated, the image resolution of the system is different than that of a conventional system with the same numerical aperture and the same wavelength. As stated by the celebrated Rayleigh resolution criterion [63], the transverse resolution is essentially the ability to resolve two close spots on the image plane, each of which is an image of a different object point. Consequently, for any examined imager of a numerical aperture identical to that of a conventional imager, when the Lagrange invariant is violated, the resolution of the two imagers is essentially dissimilar. Moreover, if, in some system, the ratio of the gap between the spots magnification and the width magnification of the spots (a figure which is termed magnification-ratio) is greater than 1, the separation between the two spots is magnified more than their widths. Therefore, the transverse resolution is enhanced in comparison to the conventional imager, because it is easier to separate the spots when the gap between them is magnified more than their widths.

Apparently, if two interfering waves, emitted from a single object point, perfectly overlap on the camera plane, the Lagrange invariant is violated in a way that maximizes the transverse resolution [4]. Therefore, the separation between any two imaged spots is magnified twofold than the width of each spot, or in other words the ratio between the transverse magnification M_T and the spot magnification M_W is 2. To show this result, we derive the expressions of the two magnifications. The transverse magnification M_T is directly obtained from (2) as

$$M_T = \frac{z_h}{f_o} \quad (3)$$

which is a general result of any configuration of FINCH. To derive the spot magnification M_W , one needs to calculate the hologram distribution of the setup as shown in Fig. 2, where a source point is located at the origin of the front focal plane of L_o . The hologram is obtained from interference between two spherical waves, one diverging from a_1 , a distance of $z_h - f_d$ from the CCD, while the other converging to a_2 , a distance of $f_c - z_h$ behind the CCD plane, where f_d is the effective focal distances of the lens L_c with the diffractive lens displayed on the SLM and f_c is the focal length of the lens L_c . Therefore, the hologram of the source point is

$$\begin{aligned} h(x, y) = & I_s(x_s, y_s) \left| \exp \left[\frac{-j\pi(x^2 + y^2)}{\lambda(z_h - f_d)} \right] \right. \\ & \left. + \exp \left[\frac{j\pi(x^2 + y^2)}{\lambda(f_c - z_h)} \right] \right|^2 = 2I_s(x_s, y_s) \\ & \times \left[1 + \cos \left\{ \left[\frac{\pi(f_c - f_d)(x^2 + y^2)}{\lambda(z_h - f_d)(f_c - z_h)} \right] \right\} \right]. \quad (4) \end{aligned}$$

One conclusion from (4) is that the reconstructed distance z_r from the hologram to the image is

$$z_r = \frac{(z_h - f_d)(f_c - z_h)}{(f_c - f_d)}. \quad (5)$$

To calculate the spot magnification, one needs two more parameters, one is the distance z_h from the SLM to the CCD in terms of f_d and f_c under the perfect overlap condition. It is easy to see that under this condition, z_h should satisfy the following relation:

$$z_h = \frac{2f_d f_c}{f_c + f_d}. \quad (6)$$

The last parameter needed here for calculating the spot magnification is the ratio between the hologram and the SLM aperture radii, R_H and R_{SLM} , respectively, which based on Fig. 2, is given by

$$\frac{R_H}{R_{SLM}} = \frac{f_c - z_h}{f_c}. \quad (7)$$

In general, a spot width is proportional to the ratio between the distance from the spot to the system aperture and the aperture radius. Therefore, the spot magnification M_W is

$$M_W = \frac{z_r/R_H}{f_o/R_{SLM}}. \quad (8)$$

Substituting (5)–(7) into (8) yields

$$M_W = \frac{z_h}{2f_o}. \quad (9)$$

Finally, based on (3) and (9), the magnification ratio is

$$\frac{M_T}{M_W} = \frac{z_h/f_o}{z_h/2f_o} = 2. \quad (10)$$

In this case, shown in Fig. 2, the Lagrange invariant is violated since both beams, emitted from each object point, contain the information on the lateral location of this point. The lateral position of a point is encoded into the linear phase of both waves. Consequently, both beams have the same linear phase with constants relative to the lateral position of the object point. In the interference event, the two linear phases of the two beams are added up constructively, in the most efficient way, only if the overlap condition between the beam projections is fulfilled. Furthermore, when the linear phases are constructively summed, the constants of the resulting linear phase are multiplied by a factor of 2 relatively to the original linear phases. In the image reconstruction stage, this resulting linear phase is translated back to a transverse image location magnified by a factor of 2 in comparison to a conventional imager. The magnification of the spot width, on the other hand, is not influenced by the extra information carried by the interfering beams, since the size of the image spot is governed by the size of the overlap between the two projections of the beams. The above-mentioned linear phases do not influence the size of the overlap.

To summarize so far, one may argue that the super resolution of FINCH is achieved because the object is observed by two different imaging systems simultaneously. It is natural and intuitive that one can get more information, and consequently better resolution, from two images of the same object captured by two different systems, than from only a single captured image. However, the dual observation is necessary to obtain a super-resolving system, but it is not enough. The additional condition for resolving better is that for every object point there should be a perfect overlap on the camera plane between the two beams. Only under this condition, can FINCH use the two images in an optimal way, in order to maximally improve the imaging resolution.

As is lengthily discussed in [4], when the above-mentioned overlap condition is satisfied, an enhancement of the transverse resolution by a factor of 2 is achieved with FINCH in comparison to conventional coherent imagers and by a factor of about 1.5 in comparison to conventional incoherent imagers. Note that this superiority of FINCH does not violate any well-known resolution limit, since FINCH is an incoherent imaging system in which the spatial bandwidth is double than that of coherent systems [63]. The resolution enhancement by a factor of about 1.5 of FINCH in comparison to conventional incoherent imagers is not realized by widening the bandwidth, but because the transfer function of FINCH is more uniform than the well-known cone-like shape of the incoherent transfer function [4]. Consequently, the above-mentioned superiority of FINCH over coherent and incoherent imagers is well established in the frame of the diffraction theory.

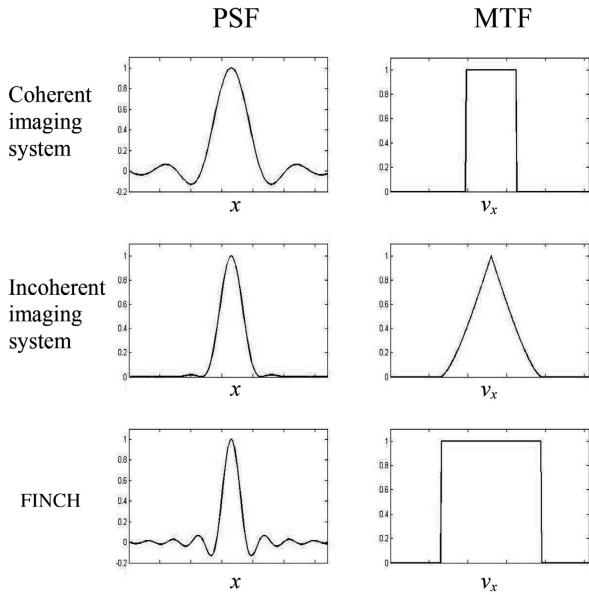


Fig. 4. Summary of the main properties of the three imaging systems discussed in the text. x and ν_x are the spatial and the spatial-frequency coordinates, respectively.

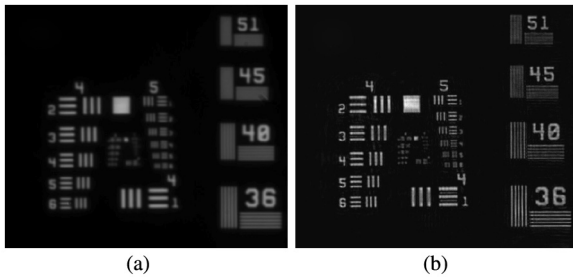


Fig. 5. Representative resolution chart images captured in (a) standard two-lens imager and (b) optimized FINCH. Both images were taken with the same numerical aperture.

In summary, FINCH resolves better than both coherent and incoherent classical imagers. Actually, FINCH has advantages from both imagers of the same numerical aperture; it has a uniform modulation transfer function (MTF) similar to a coherent imager and a cutoff frequency of an incoherent imager. Fig. 4 presents the main features of FINCH in comparison to either coherent or incoherent imagers. According to Fig. 4, FINCH is linear in the intensity but its PSF can be a complex-valued function. Its MTF follows the form of the system aperture, but the cutoff frequency can be double than that of a classical coherent imager with the same numerical aperture. In comparison to a classical incoherent imager, both systems have the same bandwidth, but the intensity of high spatial frequencies is not attenuated in FINCH as it happens in classical incoherent imagers.

A comparison between the resolution performances of a conventional two-lens imager and FINCH is shown in Fig. 5. The lateral resolution of FINCH is better than that of the two-lens imager as is reflected from Fig. 5(a) and (b), where the images are in focus, but the smaller details are better revealed in the holographic reconstructions than in the image from the two-lens imager.

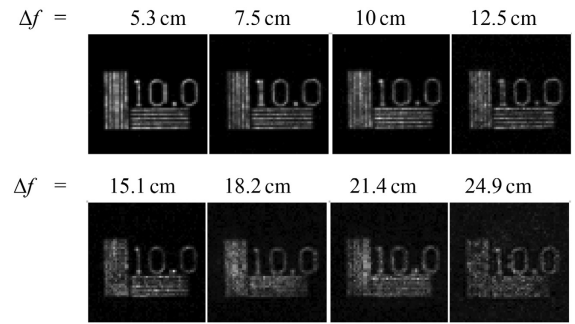


Fig. 6. Best in-focus reconstructed images from holograms captured by FINCH with different values of the gap between the two foci, Δf [59].

D. Problem of the OPD in FINCH

According to the theory of temporal coherence [63], the visibility of the interference pattern of an interferometer, like FINCH, is equal to the magnitude of the complex degree of coherence. Moreover, the visibility value goes to zero as the OPD between the interfering beams increases. According to the Wiener–Khinchine theorem, the power spectral density of the light source is the Fourier transform of the temporal coherence function [63]. Therefore, for a given light source bandwidth, the hologram visibility is higher as much as the OPD is shorter. Thus, FINCH is a spatially incoherent system which can function well only above some level of temporal coherence.

In the early days of FINCH [4], with the setup of a single diffractive lens and the constant phase mask, like in Fig. 1, and under the condition of beam overlap mentioned in the previous section, the average OPD in the system was sometimes longer than the coherence length of the given sources. Therefore, in order to get a hologram with an acceptable interference visibility, either the following acts were carried: to increase the temporal coherence, the source bandwidth was narrowed by a chromatic filter; in order to reduce the OPD, the SLM-CCD distance was increased. Clearly, both actions have high costs which can be avoided using a dual-lens FINCH [59]. The term dual-lens FINCH means that for every object, there are two images created by two different effective lenses. Fig. 2 shows an example of a dual-lens FINCH in which the condition of beam overlap is applied. The dual-lens FINCH has the advantage that its maximum OPD is smaller than that of a single-lens FINCH system. Moreover, this OPD becomes smaller as the distance between the two foci of the lenses is reduced. As a result of using dual-lens FINCH, the values of the SLM-camera distance can be considerably shortened and the source bandwidth can be significantly expanded, in comparison to the early setups [4].

The theoretical prediction that the quality of the reconstructed image is improved by narrowing the gap between the two foci applied to the SLM was tested in [59] and the results are summarized in the following. The best in-focus reconstructed planes, computed by a Fresnel back-propagation, for each of the eight values of the gap Δf between the two foci are depicted in Fig. 6. It can be seen in Fig. 6, that there is a consecutive enhancement in the reconstruction quality with reducing the gap Δf between the two foci of the two diffractive

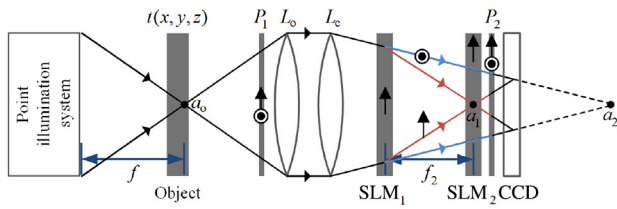


Fig. 7. Schematic of a confocal FINCH system: P_1 and P_2 , polarizers; L_o , objective lens; L_c , converging lens; SLM_1 and SLM_2 , spatial light modulators; CCD, charge-coupled device. Figure adapted from [62].

lenses. This result validates the prediction that reducing the OPD in the FINCH system increases the quality of the recorded holograms.

Once the source bandwidth and the SLM-camera distance (and consequently, the image magnification) are given, the upper limit on the value of the gap between the two foci can be easily calculated [59]. Working in the range below this upper limit guarantees relatively high temporal coherence and consequently high fringe visibility for the recorded holograms.

E. Confocal FINCH

The concept of confocal microscopy was developed by Minsky, 60 years ago [65], and has been incorporated to incoherent [66], [67] and coherent [68]–[70] holography systems, a few decades later. In standard microscopy, the quality of in-focus objects may be deteriorated by information from out-of-focus objects. This situation is especially limiting when thick samples are considered. Minsky’s confocal solution incorporates two means to mitigate this problem.

- 1) The object point of interest is selectively illuminated.
- 2) Image information from out-of-focus image points is mostly blocked by an opaque screen, whereas information from the image point of interest freely reaches the detector through a pinhole.

This elegant solution is not without costs, as target scanning is needed in order to image an entire object. Recently, a motionless confocal configuration of FINCH was presented as a solution to the problem of relatively low axial resolution of FINCH [62]. Several months after the appearance of [62], another confocal FINCH was proposed, combining the standard FINCH with a spinning disk [71]. The uniqueness of the confocal FINCH of [62] lies in its ability to perform optical sectioning of the recorded scene in a motionless manner and with the inherent super-resolution capabilities of the conventional FINCH. Hence, it is capable of imaging different planes of interest, at various depths, while suppressing information from other planes. In this manner, the axial resolution of the system is improved and details that would otherwise be lost are revealed.

The integration of these optical sectioning capabilities into FINCH has been enabled through the incorporation of an optical element termed a phase pinhole. The phase pinhole is an SLM-implemented component that imitates an actual absorbing pinhole, but at the same time allows the formation of a FINCH hologram for a specific point of interest in the observed target. The confocal FINCH system is shown in Fig. 7. The setup

is similar to the dual-lens FINCH (Fig. 2) with the addition of a second SLM, SLM_2 , positioned in the transverse plane in which the image point a_1 is formed. A diffractive optical element, consisting of a negative (diverging) axicon that surrounds a small circular area of uniform phase modulation, hereby referred to as a phase pinhole, is displayed on SLM_2 . For every scanning point a_o , the phase at the pinhole region is set to three different phase values for the three acquired holograms, usually 0° , 120° , and 240° , while on SLM_1 , the same diffractive pattern is displayed during the acquisition of a single image section. Since the phase is altered only within the phase pinhole, any pattern carried by waves that pass through SLM_2 outside the phase pinhole is lost after the phase-shifting process. Generally, the phase pinhole can be thought of as a standard pinhole for the polarization components parallel to the active axis of SLM_2 and as a transparent aperture for the orthogonal polarization components. The information recorded by the process is only the pattern encoded into the interference between waves that pass through the phase pinhole of SLM_2 , and its orthogonal counterpart imaged at the point a_2 .

The incorporation of a phase pinhole into FINCH, as described above, is sufficient to achieve optical sectioning. However, better sectioning results can be achieved by the formation of a complete confocal FINCH system (Fig. 7) through the incorporation of a point illumination system. Similar to Minsky’s solution, any of the object points that are outside the cone of light will not be recorded. Thus, there are two mechanisms working together to allow optical sectioning. Obviously, since only a single point in space is properly imaged, a scanning mechanism is needed to record the complete object. This is in contrast to a regular FINCH hologram in which the complete 3-D information of the wide-field illuminated scene is encoded. Luckily, scanning of the entire object can be performed electronically, without any mechanical movements [62].

In the sectioning experiments, the results of a regular FINCH and a sectioning FINCH were compared. The regular FINCH was realized on the setup of Fig. 7 by setting the phase mask of SLM_2 into a constant zero modulation, and in both systems, the proposed point illumination excluded, so that the contribution of the phase pinhole displayed on SLM_2 is highlighted. We consider the phase pinhole as a novel part in the system, as scanning illumination systems are commonly used in confocal microscopy [68]–[70]. Note that sectioning implemented only by the phase pinhole can be useful for circumstances in which the observed scene cannot be selectively illuminated. The experimental results are shown in Fig. 8. Reconstructions from conventional FINCH holograms of two resolution charts, at the plane close to, and far from, the objective are depicted in Fig. 8(a) and (b), respectively. It is clear that the out-of-focus images extremely disrupt the reconstructions. The equivalents of Fig. 8(a) and (b) for the reconstruction of the sectioning FINCH are shown in Fig. 8(c) and (d), respectively. Here, the out-of-focus images are highly diminished, and the in-focus images clearly appear with improved contrast, complete details, and low background noise. The optical sectioning capabilities of the proposed system are thus verified, and are expected to be improved even further once a point illumination is incorporated.

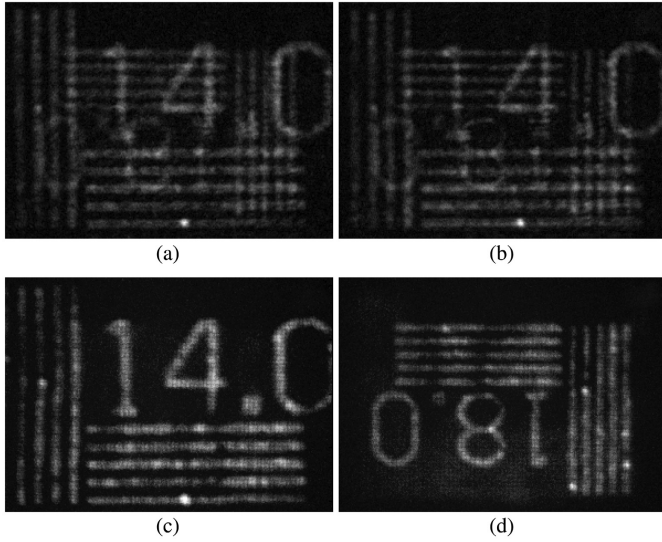


Fig. 8. Experimental results. (a) FINCH reconstruction of a 14.0 cycles/mm resolution chart located 30 cm. (b) FINCH reconstruction of a 18.0 cycles/mm resolution chart located 31-cm away from the objective lens. (c) and (d) are the optical-sectioning-FINCH equivalents of (a) and (b), respectively.

Overall, the confocal configuration of FINCH can efficiently suppress out-of-focus information from a FINCH-recorded hologram combining the high lateral resolution of FINCH and the optical sectioning features of confocal microscopy. We believe that this system is of special importance for establishing a firm place for FINCH in biological microscopy.

III. FOURIER INCOHERENT SINGLE CHANNEL HOLOGRAPHY

As mentioned in Section II, a single FINCH hologram contains the complete 3-D information of an object. Yet, at least three images are required to solve the twin-image problem. The FISCH system can overcome this problem by recording a single cosine Fourier hologram [72], [73]. Thus, a single exposure, rather than three as in FINCH, can yield the desired hologram from which an object can be reconstructed with enough separation between the various diffraction orders and without an overlap of the twin-image. Moreover, FISCH may exploit other beneficial qualities of Fourier holograms over Fresnel holograms including: enhanced robustness to information loss due to the distribution of information from each object point over the entire hologram plane and easier filtering ability that results from capturing a hologram in the spatial frequency domain. Concurrently, FISCH maintains other beneficial characteristics of FINCH, including its inherent super-resolution property [73], meaning that just like FINCH, FISCH also offers a resolution improvement of up to a factor of two when compared with standard coherent imaging systems of a similar numerical aperture.

Following the initial presentation of FISCH [72], a Sagnac radial shearing interferometer-based system was introduced as a system for recording spatially incoherent digital Fourier holograms [74]. Since then, a design based on similar concepts, using a triangular radial shearing interferometer has appeared [75], [76]. A common feature of these works is the formation

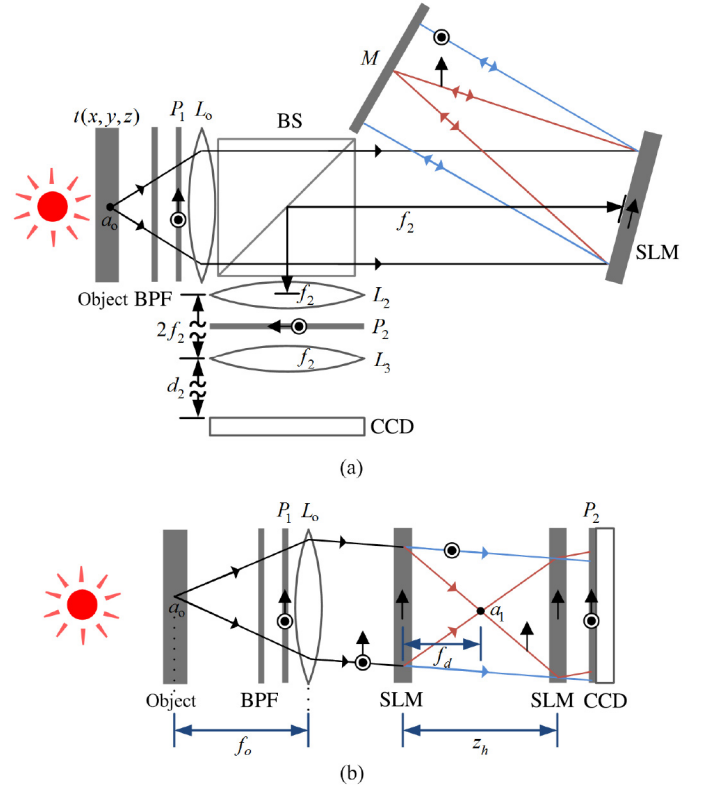


Fig. 9. (a) Experimental setup and (b) simplified schematic. Schematics of the first FISCH recorder [72]: BPF, band pass filter; P_1 and P_2 , polarizers; L_o , objective lens; BS, beam splitter; SLM, spatial light modulator; M , mirror; L_2 and L_3 , lenses; CCD, charge-coupled device.

of a Fourier hologram through the interference of two radially sheared wavefronts. Fairly recently, a dual channel rotational shearing interferometer (RSI) has been proposed [77].

A. Single SLM-Based Design

A schematic illustration of the first FISCH recorder [72] is given in Fig. 9(a). Under spatially incoherent illumination, it is assumed that any two points of a 3-D object are uncorrelated and, therefore, cannot produce an interference pattern. In FISCH, however, each input point is doubled in such a manner that allows the formation of a fringe pattern. The overlapping fringe patterns that are induced by all object points are captured by a digital camera. These patterns encode the point positions in space, implying that the information from all points is captured by a single exposure. FISCH is built around a phase-only SLM that is sensitive to polarization, meaning that the SLM has orthogonal active and nonactive axes. For polarization components that are oriented along the active axis, the SLM acts as a diffractive lens and for polarization components that are oriented along the nonactive axis, the SLM acts merely as a mirror. Beam diagrams for the active and nonactive axes of the SLMs in FISCH are shown in Fig. 9(b), demonstrating a 180° rotational shearing interference that occurs for a point source object that lies within the front focal plane of the objective lens L_o . Note that in Fig. 9(b) two transmissive SLMs are shown, for simplicity. The actual optical setup uses only one reflective SLM, in a double-pass mode, as shown in Fig. 9(a). Ideally, the distance

d_2 is chosen to be equal to f_2 , by forming a relay system that comprised two lenses L_2 and L_3 , setting the effective distance between the CCD and the SLM to zero. Further, note that the polarization method of multiplexing, previously described for FINCH, is essential in FISCH.

The distribution of the recorded hologram is obtained by observing the camera intensity distribution caused by a single point source. Knowing the hologram of a single point, the complete hologram is a summation over all the camera intensity distributions, each of which is caused by a different point of the object. For the specific case of a source point located on the front focal plane of lens L_o of Fig. 9, at an arbitrary lateral location $\bar{r}_s = (x_s, y_s)$, the intensity on the CCD plane results from the interference of two slanted plane waves, one originated from the source point a_o and the other from the point a_1 . The plane wave originated from the source is tilted by the angles $(\theta_{1,x}, \theta_{1,y}) = [-\arctan(x_s/f_o), -\arctan(y_s/f_o)]$, where the other plane wave is tilted by $(\theta_{2,x}, \theta_{2,y}) = \{\arctan[(x_s f_d/f_o)/f_d], \arctan[(y_s f_d/f_o)/f_d]\} = [\arctan(x_s/f_o), \arctan(y_s/f_o)]$, where f_d is the focal length of the diffractive lens displayed on the SLM. Therefore, the expression of a hologram recorded from a single object point is

$$\begin{aligned} h(x, y) &= I_s(x_s, y_s) \\ &\times \left| \exp \left[\frac{-j2\pi(x_s x + y_s y)}{\lambda f_o} \right] + \exp \left[\frac{j2\pi(x_s x + y_s y)}{\lambda f_o} \right] \right|^2 \\ &= 2I_s(x_s, y_s) \left\{ 1 + \cos \left[\frac{4\pi(x_s x + y_s y)}{\lambda f_o} \right] \right\}. \end{aligned} \quad (11)$$

The complete hologram, for the above case, is an integral over all the object distribution as follows:

$$H(x, y) = I_o + 2 \iint I_s(x_s, y_s) \cos \left[\frac{4\pi(x_s x + y_s y)}{\lambda f_o} \right] dx_s dy_s. \quad (12)$$

The second term of (12) is the expression of a Cosine-Fourier transform of the object intensity $I_s(x_s, y_s)$. Therefore, this kind of hologram is termed as Fourier hologram. In order to reconstruct an image from this hologram, one needs to numerically Fourier transform the hologram.

Experimental results [72] from a FISCH system based on Fig. 9(a) are presented in Fig. 10. First, a hologram was recorded with a resolution chart located at the front focal plane of the objective lens L_o . It was then digitally reconstructed by simple calculation of the inverse 2-D Fourier transform of the recorded hologram. The result, shown in Fig. 10(a), clearly demonstrates that most of the information from the object can be extracted from a single exposure. However, the bias term is quite dominant in the reconstruction and reduces the quality of the reconstruction. By taking a second exposure with a 180° total phase-shift in the SLM-modulated beam, most of the bias can be removed, as shown in Fig. 10(b). Fig. 10(c) and (d) demonstrates the system capability of maintaining 3-D information, where the hologram was recorded with the resolution chart moved several centimeters away from its previous position. This time, the reconstruction was performed optically using a simple array that consists of a collimated laser

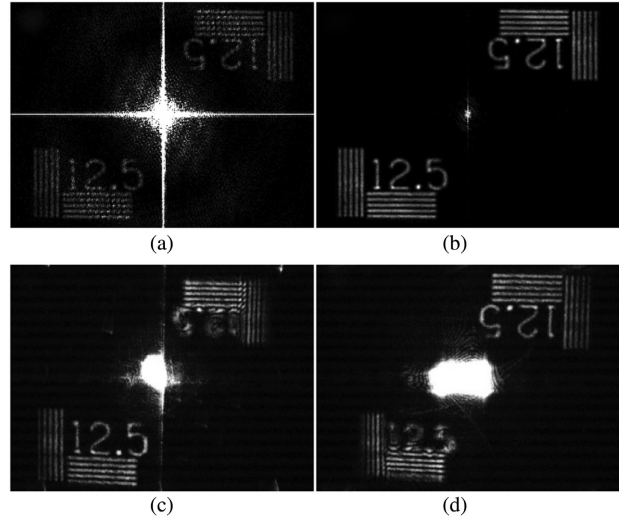


Fig. 10. Experimental results from a FISCH recorder based on the schematic of Fig. 9(a). (a) Digital hologram reconstruction of a single exposure hologram, with the target located at the front focal plane of the objective lens. (b) Digital hologram reconstruction of a dual exposure hologram, where a 180° phase-shifting was used to remove most of the bias term that is visible in (a). (c) Optical reconstruction of a dual exposure hologram, with the target located several centimeters in front of the objective lens front focal plane. (d) Optical reconstruction of the twin-image of (c). Figure adapted from [72].

beam, an amplitude modulating SLM used to display the dual exposure hologram, a Fourier transforming lens, and a camera that moved along the z -axis used to capture either the image of the resolution chart [Fig. 10(c)] or its twin [Fig. 10(d)].

B. Two SLMs-Based Design

An enhanced version of FISCH, with a shorter OPD than the first FISCH [72], was introduced in [73]. The reduction in OPD is of high importance, allowing the enhanced FISCH system to efficiently handle signals with wider bandwidths. However, unlike the original FISCH design [72], where it was possible to implement the system with a single SLM in a double-pass mode [Fig. 9(a)], the newer design, depicted in Fig. 11, actually requires two different SLMs, as the diffractive elements displayed upon the SLMs are different. Still, this apparent disadvantage proves very useful when the resemblance between FISCH and FINCH (Fig. 2) is observed. By electronically controlling SLM₂, the enhanced FISCH system can instantaneously be switched into a FINCH system and vice versa, enabling the recording of both Fourier and Fresnel spatially incoherent digital holograms.

The enhanced FISCH system is schematically presented in Fig. 11. The configuration resembles the one of Fig. 9, but two differences are prominent: an additional converging lens L_c is located between L_o and the first SLM; two SLMs are now used and are placed with their active axes perpendicular to each other and at a 45° angle to the transmission axis of the polarizers. This configuration enables separate control over the orthogonal polarization components of the light beam traveling within the FISCH system. In Fig. 11, a spherical wave is induced from the point source a_o and is collimated into a plane wave by the lens L_o . It is then converged into a

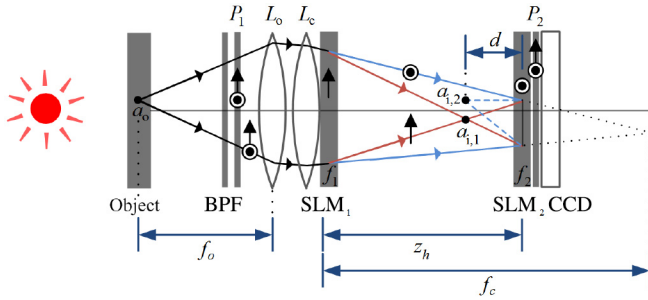


Fig. 11. Schematic of an enhanced FISCH recorder [73]: BPF, band-pass filter; P_1 and P_2 , polarizers; L_o , objective lens; L_c , converging lens; SLM₁ and SLM₂, spatial light modulators; CCD, charge-coupled device. The polarization sensitive axes of the SLMs are perpendicular to each other.

spherical wave by the lens L_c . This wave is transformed into two diverging beam cones: 1) one from the real image point $a_{i,1}$, influenced by SLM₁ (on which a phase mask of a converging diffractive lens is displayed); and 2) the other from the virtual image point $a_{i,2}$, influenced by SLM₂ (on which a diverging diffractive lens is displayed). The focal lengths of the two SLM-realized lenses are set in a manner that assures that these two beams completely overlap at the plane of SLM₂. This plane is also shared by the CCD, where a relay system (not shown in the figure) is used. The two beam cones originate from the same point source and can thus interfere, granted that the OPD between the two is small enough. For the point a_o , a cosine fringe pattern is captured by the digital camera, representing the source lateral position. For other points that are located outside of the front focal plane of the objective lens, the two image points are no longer formed at equal z -distances from SLM₁. In turn, the longitudinal gap between the image points leads to a quadratic phase term, representing the depth location of the source, which is encoded into the fringe pattern. Like in FINCH, fringe patterns of all spatially incoherent point sources are summed over the camera. However, here a Fourier hologram is formed because one image point is 180° rotated compared to the other. This strongly resembles that case of the RSI [77]. Still, in contrast to RSI, FISCH can store 3-D information. In a sense, FISCH is actually a combination of both rotational and radial shearing interferometers.

The mathematical expression of the enhanced FISCH can be easily obtained by looking on the scheme shown in Fig. 11. The recorded hologram of a point source a_o is the intensity distribution of the interference between two declined spherical waves originated from the two points $a_{i,1}$ and $a_{i,2}$ located at an axial distance d before SLM₂ and at the transverse points $\bar{r}_{i,1}$ and $\bar{r}_{i,2}$, respectively. d , $\bar{r}_{i,1}$, and $\bar{r}_{i,2}$ are calculated by the imaging equations of spherical lenses, as follows:

$$\frac{1}{d} = \frac{1}{f_2} - \frac{1}{f_c - z_h}; \quad \bar{r}_{i,1} = \frac{-\bar{r}_s f_c f_1}{f_o (f_c + f_1)}; \quad (13)$$

$$\bar{r}_{i,2} = \frac{\bar{r}_s f_c d}{f_o (f_c - z_h)}$$

where z_h is the gap between the two SLMs and f_c, f_1 , and f_2 are the focal distances of the lens L_c , the lens on SLM₁ and

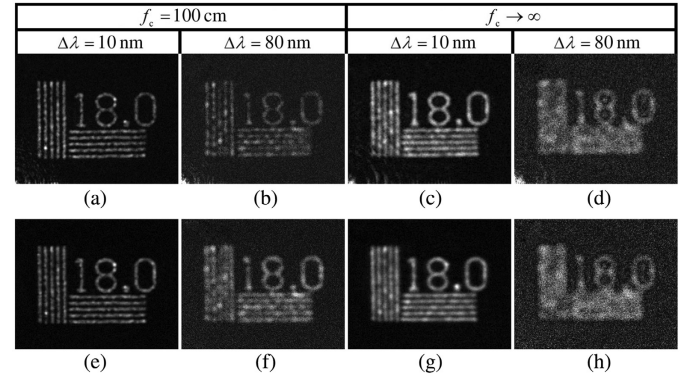


Fig. 12. Effect of bandwidth and OPD on FISCH (a–d) and FINCH (e–h) resolution: (a, e) with $f_c = 100$ cm and a 10-nm FWHM light source, where all details of the RC are clearly visible; (b, f) with $f_c = 100$ cm and a 80-nm FWHM light source, where the reconstruction quality is diminished, but most details of the RC are still visible; (c, g) with $f_c \rightarrow \infty$ and a 10-nm FWHM light source, where most details of the RC are clearly visible but less clear than (a, e); and (d, h) with $f_c \rightarrow \infty$ and a 80-nm FWHM light source, where most details of the RC are lost. Figure adapted from [73].

the lens on SLM₂, respectively. Knowing all the parameters of the two points $a_{i,1}$ and $a_{i,2}$ enables to formulate the recorded hologram of a single source point as the interference intensity of spherical waves originated from these two points, as follows:

$$h(x, y) = I_s(x_s, y_s) \left| \exp \left\{ \frac{j\pi}{\lambda d} \left[(x - x_{i,1})^2 + (y - y_{i,1})^2 \right] \right\} + \exp \left\{ \frac{j\pi}{\lambda d} \left[(x - x_{i,2})^2 + (y - y_{i,2})^2 \right] \right\} \right|^2 = 2I_s(x_s, y_s) \times \left\{ 1 + \cos \left[\frac{4\pi(x_{i,1}x + y_{i,1}y)}{\lambda d} \right] \right\}. \quad (14)$$

As in the case of the single-SLM FISCH, the complete hologram is an integral over all the object distribution as follows:

$$H(x, y) = I_o + 2 \iint I_s(x_s, y_s) \cos \left[\frac{4\pi(x_{i,1}x + y_{i,1}y)}{\lambda d} \right] dx_s dy_s. \quad (15)$$

The second term of (15) has the same form of the second term of (12), which is the expression of Cosine-Fourier transform of the object intensity $I_s(x_s, y_s)$, and therefore this hologram is also a Fourier hologram.

The reduction in the maximal OPD between the two FISCH systems [72], [73] is analytically derived in [73]. To demonstrate the advantages of the suggested FISCH design due to this reduction, a set of experiments [73] is described in the following. A single NBS 1963A resolution chart, located at the objective front focal plane, was illuminated either with a 10-nm full-width half-max (FWHM) light source, or with an 80-nm FWHM light source. The system was tested with and without the converging lens L_c . The ratio between the values of maximal OPD with and without L_c is 2.74/5, implying that the reduction in OPD due to the enhanced design, in this particular case, is close to 50%. The experimental results are presented in

Fig. 12(a)–(d). With $\Delta\lambda = 10$ nm, both FISCH configurations demonstrate sufficient resolution to show complete details of the 18 line pairs per mm target [Fig. 12(a) and (c)]. Once the bandwidth of the illumination is broadened to $\Delta\lambda = 80$ nm, both configurations exhibit deterioration of the reconstruction quality [Fig. 12(b) and (d)]. Yet, while with $f_c \rightarrow \infty$ (without L_c , nonenhanced FISCH) details are lost as the grating lines are smeared into a rectangle, with $f_c = 100$ cm (enhanced FISCH), details are preserved and lines are separable. Thus, the enhanced resolution of the proposed design, due to the reduced OPD, is demonstrated. The same behavior of OPD sensitivity exists in FINCH as well, as demonstrated in Fig. 12(e)–(h). Note that in the presented FINCH experiments [Fig. 12(e)–(h)], a complete phase-shifting procedure was performed to eliminate the bias and twin-image terms, whereas in FISCH [Fig. 12(a)–(d)] only two exposures with a 180° total phase-shift were recorded, so that most of the bias term could be removed.

Comparing the two FISCH systems, it is interesting to note that in the single SLM FISCH [72] of Fig. 9 the interference happens between two plane waves, thus effectively the two opposite point images are obtained in the infinity. On the other hand, in the dual-lens FISCH [73] of Fig. 11, the interference happens between two quadratic waves, thus the two opposite point images are located nearby the hologram plane. The combination of FISCH inherent robustness together with its capability of recording single exposure holograms under incoherent illumination holds great potential for many possible applications.

IV. CONCLUSION

Two families of incoherent hologram recorders have been reviewed in this paper, FINCH and FISCH. These two systems are considered as imaging systems. As so, they should be optimized to produce the best possible images. The main imaging aspect considered in the reviewed research is the lateral imaging resolution. For the two incoherent hologram recorders, exact conditions for achieving optimal resolution have been discussed and this optimal resolution has been proved to be better than that of classical coherent and incoherent imagers. These fundamental conclusions are valid for other similar incoherent hologram recorders [5], [8], [9], [23]–[59], and therefore, are important and general beyond FINCH and FISCH alone.

Besides the issue of optimal lateral resolution, other topics should be considered. The topics mentioned herein are as follow.

- 1) Reduce the OPD using the dual-lens multiplexing method in FINCH, or by introducing two SLMs in FISCH. Shortening the OPD enables working with light sources of a wider bandwidth.
- 2) Reduce the noise in the output images by multiplexing the two interferometric channels using two orthogonal polarizations, a method which has been implemented in both incoherent hologram recorders FINCH, FISCH, and recently extended to coherent recorders as well [17], [20].
- 3) Improve the axial resolution using the confocal version of FINCH.

- 4) Reduce the number of exposures during the hologram capturing process in FISCH by working with an off-axis hologram recorder.

These and other issues should be further improved in order to utilize these and similar systems for the various applications mentioned in this paper.

ACKNOWLEDGMENT

The authors would like to thank the persons with whom they had the honor to collaborate in the various works presented in this review paper. Especially, they wish to thank G. Brooker, B. Katz, and N. Siegel.

REFERENCES

- [1] U. Schnars and W. Jueptner, *Digital Holography*. Berlin, Germany: Springer-Verlag, 2005, ch. 3.
- [2] E. Cuhe, F. Bevilacqua, and C. Depeursinge, "Digital holography for quantitative phase-contrast imaging," *Opt. Lett.*, vol. 24, no. 5, pp. 291–293, Mar. 1999.
- [3] P. Girshovitz and N. T. Shaked, "Real-time quantitative phase reconstruction in off-axis digital holography using multiplexing," *Opt. Lett.*, vol. 39, no. 8, pp. 2262–2265, Apr. 2014.
- [4] J. Rosen, N. Siegel, and G. Brooker, "Theoretical and experimental demonstration of resolution beyond the Rayleigh limit by FINCH fluorescence microscopic imaging," *Opt. Express*, vol. 19, no. 27, pp. 26249–26268, Dec. 2011.
- [5] D. Weigel, H. Babovsky, A. Kiessling, and R. Kowarschik, "Widefield microscopy with infinite depth of field and enhanced lateral resolution based on an image inverting interferometer," *Opt. Commun.*, vol. 342, pp. 102–108, May 2015.
- [6] V. Mico, Z. Zalevsky, P. García-Martínez, and J. García, "Superresolved imaging in digital holography by superposition of tilted wavefronts," *Appl. Opt.*, vol. 45, no. 5, pp. 822–828, Aug. 2006.
- [7] G. Indebetouw, Y. Tada, J. Rosen, and G. Brooker, "Scanning holographic microscopy with resolution exceeding the Rayleigh limit of the objective by superposition of off-axis holograms," *Appl. Opt.*, vol. 46, no. 6, pp. 993–1000, Feb. 2007.
- [8] M. K. Kim, "Adaptive optics by incoherent digital holography," *Opt. Lett.*, vol. 37, no. 13, pp. 2694–2696, Jul. 2012.
- [9] M. K. Kim, "Incoherent digital holographic adaptive optics," *Appl. Opt.*, vol. 52, no. 1, pp. A117–A130, Jan. 2013.
- [10] J. Maycock, C. P. McElhinney, B. M. Hennelly, T. J. Naughton, J. B. McDonald, and B. Javidi, "Reconstruction of partially occluded objects encoded in three-dimensional scenes by using digital holograms," *Appl. Opt.*, vol. 45, no. 13, pp. 2975–2985, May 2006.
- [11] Y. Rivenson, A. Rot, S. Balber, A. Stern, and J. Rosen, "Recovery of partially occluded objects by applying compressive Fresnel holography," *Opt. Lett.*, vol. 37, no. 10, pp. 1757–1759, May 2012.
- [12] P. Bouchal and Z. Bouchal, "Selective edge enhancement in three-dimensional vortex imaging with incoherent light," *Opt. Lett.*, vol. 37, no. 14, pp. 2949–2951, Jul. 2012.
- [13] Y. Pan *et al.*, "Edge extraction using a time-varying vortex beam in incoherent digital holography," *Opt. Lett.*, vol. 39, no. 14, pp. 4176–4179, Jul. 2014.
- [14] G. Indebetouw, "Scanning holographic microscopy with spatially incoherent sources: reconciling the holographic advantage with the sectioning advantage," *J. Opt. Soc. Amer. A*, vol. 26, no. 2, pp. 252–258, Feb. 2009.
- [15] Y.-C. Lin, C.-J. Cheng, and T.-C. Poon, "Optical sectioning with a low-coherence phase-shifting digital holographic microscope," *Appl. Opt.*, vol. 50, no. 7, pp. B25–B30, Mar. 2011.
- [16] V. Mico, Z. Zalevsky, and J. Garcia, "Superresolution optical system by common-path interferometry," *Opt. Express*, vol. 14, no. 12, pp. 5168–5177, Jun. 2006.
- [17] Y. Rivenson, B. Katz, R. Kelner, and J. Rosen, "Single channel in-line multi-modal digital holography," *Opt. Lett.*, vol. 38, no. 22, pp. 4719–4722, Nov. 2013.
- [18] S. Seo, T.-W. Su, D. K. Tseng, A. Erlinger, and A. Ozcan, "Lensfree holographic imaging for on-chip cytometry and diagnostics," *Lab Chip*, vol. 9, no. 6, pp. 777–787, Jan. 2009.

- [19] O. Mudanyali *et al.*, "Compact, light-weight and cost-effective microscope based on lensless incoherent holography for telemedicine applications," *Lab Chip*, vol. 10, no. 11, pp. 1417–1428, 2010.
- [20] R. Kelner, B. Katz, and J. Rosen, "Common path in-line holography using enhanced joint object reference digital interferometers," *Opt. Express*, vol. 22, no. 5, pp. 4995–5009, Mar. 2014.
- [21] T.-C. Poon, K. B. Doh, B. W. Schilling, M. H. Wu, K. K. Shinoda, and Y. Suzuki, "Three-dimensional microscopy by optical scanning holography," *Opt. Eng.*, vol. 34, pp. 1338–1344, May 1995.
- [22] N. T. Shaked, B. Katz, and J. Rosen, "Review of three-dimensional holographic imaging by multiple-viewpoint-projection based methods," *Appl. Opt.*, vol. 48, no. 34, pp. H120–H136, Dec. 2009.
- [23] G. W. Stroke and R. C. Restrick, "Holography with spatially incoherent light," *Appl. Phys. Lett.*, vol. 7, no. 9, pp. 229–231, Nov. 1965.
- [24] P. J. Peters, "Incoherent holograms with mercury light source," *Appl. Phys. Lett.*, vol. 8, no. 8, pp. 209–210, Apr. 1966.
- [25] H. R. Worthington, Jr., "Production of holograms with incoherent illumination," *J. Opt. Soc. Amer.*, vol. 56, no. 10, pp. 1397–1398, Oct. 1966.
- [26] G. Cochran, "New method of making Fresnel transforms with incoherent light," *J. Opt. Soc. Amer.*, vol. 56, no. 11, pp. 1513–1517, Nov. 1966.
- [27] J. B. Breckinridge, "Two-dimensional white light coherence interferometer," *Appl. Opt.*, vol. 13, no. 12, pp. 2760–2762, Dec. 1974.
- [28] G. Sirat and D. Psaltis, "Conoscopic holography," *Opt. Lett.*, vol. 10, no. 1, pp. 4–6 Jan. 1985.
- [29] S. Marathay, "Noncoherent-object hologram: Its reconstruction and optical processing," *J. Opt. Soc. Amer. A*, vol. 4, no. 10, pp. 1861–1868, Oct. 1987.
- [30] S.-G. Kim, B. Lee, and E.-S. Kim, "Removal of bias and the conjugate image in incoherent on-axis triangular holography and real-time reconstruction of the complex hologram," *Appl. Opt.*, vol. 36, no. 20, pp. 4784–4791, Jul. 1997.
- [31] J. Rosen and G. Brooker, "Digital spatially incoherent Fresnel holography," *Opt. Lett.*, vol. 32, no. 8, pp. 912–914, Apr. 2007.
- [32] B. Katz, D. Wulich, and J. Rosen, "Optimal noise suppression in Fresnel incoherent correlation holography (FINCH) configured for maximum imaging resolution," *Appl. Opt.*, vol. 49, no. 30, pp. 5757–5763, Oct. 2010.
- [33] P. Bouchal, J. Kapitán, R. Chmelík, and Z. Bouchal, "Point spread function and two-point resolution in Fresnel incoherent correlation holography," *Opt. Express*, vol. 19, no. 16, pp. 15603–15620, Aug. 2011.
- [34] Y. Tone, K. Nitta, O. Matoba, and Y. Awatsuji, "Analysis of reconstruction characteristics in fluorescence digital holography," in *Digital Holography and Three-Dimensional Imaging*, OSA Technical Digest (CD), Washington, DC, USA: Optical Society of America, 2011, Paper DTuC13.
- [35] X. Lai, Y. Zhao, X. Lv, Z. Zhou, and S. Zeng, "Fluorescence holography with improved signal-to-noise ratio by near image plane recording," *Opt. Lett.*, vol. 37, no. 13, pp. 2445–2447, Jul. 2012.
- [36] T. Man, Y. Wan, H. Chen, Z. Jiang, and D. Wang, "Quantitative evaluation of spatial phase light modulator characteristics in Fresnel incoherent correlation holography," *Proc. SPIE*, vol. 8556, pp. 855613-1–855613-9, Nov. 2012.
- [37] H. Chen, Y. Wan, T. Man, Z. Jiang, and D. Wang, "Effect of phase-shift step on hologram reconstruction in Fresnel incoherent correlation holography," *Proc. SPIE*, vol. 8556, pp. 85560L-1–85560L-9, Nov. 2012.
- [38] X. Lai and S. Zeng, "Optical path difference characteristics of the fluorescence holographic system," *Proc. SPIE*, vol. 8556, pp. 855617-1–855617-7, Nov. 2012.
- [39] N. Siegel, J. Rosen, and G. Brooker, "Reconstruction of objects above and below the objective focal plane with dimensional fidelity by FINCH fluorescence microscopy," *Opt. Express*, vol. 20, no. 18, pp. 19822–19835, Aug. 2012.
- [40] N. Siegel, J. Rosen, and G. Brooker, "Faithful reconstruction of digital holograms captured by FINCH using a Hamming window function in the Fresnel propagation," *Opt. Lett.*, vol. 38, no. 19, pp. 3922–3925, Oct. 2013.
- [41] X. Lai, S. Zeng, X. Lv, J. Yuan, and L. Fu, "Violation of the Lagrange invariant in an optical imaging system," *Opt. Lett.*, vol. 38, no. 11, pp. 1896–1898, Jun. 2013.
- [42] P. Bouchal and Z. Bouchal, "Concept of coherence aperture and pathways toward white light high-resolution correlation imaging," *New J. Phys.*, vol. 15, p. 123002, Dec. 2013.
- [43] K. Tsuchiya, Y. Tone, K. Nitta, O. Matoba, and Y. Awatsuji, "Influence of spatial coherence degree in fluorescence digital holography," in *Proc. 2013 Conf. Lasers Electro-Opt. Pacific Rim (CLEOPR)*, Washington, DC, USA: Optical Society of America, 2013, Paper WPF_30.
- [44] Y.-H. Wan, T.-L. Man, H. Chen, Z.-Q. Jiang, and D.-Y. Wang, "Effect of wavefront properties on numerical aperture of Fresnel hologram in incoherent holographic microscopy," *Chin. Phys. Lett.*, vol. 31, no. 4, pp. 044203–1–4, Apr. 2014.
- [45] W. Qin *et al.*, "Two-step phase-shifting fluorescence incoherent holographic microscopy," *J. Biomed. Opt.*, vol. 19, no. 6, pp. 060503:1–3, Jun. 2014.
- [46] W. Qin *et al.*, "Fast fluorescence holographic microscopy," *Proc. SPIE*, vol. 8949, pp. 89491W-1–89491W-7, Mar. 2014.
- [47] P. Bouchal and Z. Bouchal, "Non-iterative holographic axial localization using complex amplitude of diffraction-free vortices," *Opt. Express*, vol. 22, no. 24, pp. 30200–30216, Nov. 2014.
- [48] F. Zeng, J. Fan, H. Zhao, X. Lu, S. Ma, and L. Zhong, "Visual evaluation of the FINCH recording quality," *Microw. Opt. Technol. Lett.*, vol. 57, no. 6, pp. 1098–2760, Mar. 2015.
- [49] J. Rosen and G. Brooker, "Non-scanning motionless fluorescence three-dimensional holographic microscopy," *Nature Photon.*, vol. 2, pp. 190–195, Mar. 2008.
- [50] G. Brooker, N. Siegel, J. Rosen, N. Hashimoto, M. Kurihara, and A. Tanabe, "In-line FINCH super resolution digital holographic fluorescence microscopy using a high efficiency transmission liquid crystal GRIN lens," *Opt. Lett.*, vol. 38, no. 24, pp. 5264–5267, Dec. 2013.
- [51] J. Hong and M. K. Kim, "Overview of techniques applicable to self-interference incoherent digital holography," *J. Eur. Opt. Soc. Rapid Publ.*, vol. 8, pp. 13077.1–13077.8, Dec. 2013.
- [52] M. K. Kim, "Full color natural light holographic camera," *Opt. Express*, vol. 21, no. 8, pp. 9636–9642, Apr. 2013.
- [53] Y. Hayasaki, R. Abe, and T. Yanagawa, "Three-dimensional mapping of fluorescent nanoparticles using incoherent digital holography," *Opt. Lett.*, vol. 40, no. 14, pp. 3312–3315, Jul. 2015, doc. ID 240146.
- [54] P. Bouchal and Z. Bouchal, "Wide-field common-path incoherent correlation microscopy with a perfect overlapping of interfering beams," *J. Eur. Opt. Soc. Rapid Publ.*, vol. 8, pp. 13011.1–13011.8, Jan. 2013.
- [55] B. Katz and J. Rosen, "Super-resolution in incoherent optical imaging using synthetic aperture with Fresnel elements," *Opt. Express*, vol. 18, no. 2, pp. 962–972, Jan. 2010.
- [56] B. Katz and J. Rosen, "Could SAFE concept be applied for designing a new synthetic aperture telescope?," *Opt. Express*, vol. 19, no. 6, pp. 4924–4936, Mar. 2011.
- [57] Y. Kashter and J. Rosen, "Enhanced-resolution using modified configuration of Fresnel incoherent holographic recorder with synthetic aperture," *Opt. Express*, vol. 22, no. 17, pp. 20551–20565, Aug. 2014.
- [58] J. Rosen and G. Brooker, "Fluorescence incoherent color holography," *Opt. Express*, vol. 15, no. 5, pp. 2244–2250, Mar. 2007.
- [59] B. Katz, J. Rosen, R. Kelner, and G. Brooker, "Enhanced resolution and throughput of Fresnel incoherent correlation holography (FINCH) using dual diffractive lenses on a spatial light modulator (SLM)," *Opt. Express*, vol. 20, no. 8, pp. 9109–9121, Apr. 2012.
- [60] T.-C. Poon, *Optical Scanning Holography with MATLAB*. New York, NY, USA: Springer, 2007, ch. 2, p. 49.
- [61] G. Brooker, N. Siegel, V. Wang, and J. Rosen, "Optimal resolution in Fresnel incoherent correlation holographic fluorescence microscopy," *Opt. Express*, vol. 19, no. 6, pp. 5047–5062, Mar. 2011.
- [62] R. Kelner, B. Katz, and J. Rosen, "Optical sectioning using a digital Fresnel incoherent-holography-based confocal imaging system," *Optica*, vol. 1, no. 2, pp. 70–74, Aug. 2014.
- [63] M. Born and E. Wolf, in *Principles of Optics*. New York, NY, USA: Pergamon, 1980, Ch. 8.6.3, p. 419; Ch. 4.4.5, p. 165; Ch. 10.3, p. 499.
- [64] J. Rosen and R. Kelner, "Modified Lagrange invariants and their role in determining transverse and axial imaging resolutions of self-interference incoherent holographic systems," *Opt. Express*, vol. 22, no. 23, pp. 29048–29066, Nov. 2014.
- [65] M. Minsky, "Memoir on inventing the confocal scanning microscope," *Scanning*, vol. 10, no. 4, pp. 128–138, 1988.
- [66] P.-C. Sun and E. N. Leith, "Broad-source image plane holography as a confocal imaging process," *Appl. Opt.*, vol. 33, no. 4, pp. 597–602, Feb. 1994.
- [67] R. Chmelík and Z. Harna, "Parallel-mode confocal microscope," *Opt. Eng.*, vol. 38, no. 10, pp. 1635–1639, Oct. 1999.
- [68] S. Lai, R. A. McLeod, P. Jacquemin, S. Atalick, and R. Herring, "An algorithm for 3-D refractive index measurement in holographic confocal microscopy," *Ultramicroscopy*, vol. 107, no. 2–3, pp. 196–201, Mar. 2007.
- [69] S. Goy and D. Psaltis, "Digital confocal microscope," *Opt. Express*, vol. 20, no. 20, pp. 22720–22727, Sep. 2012.

- [70] C. Liu, S. Marchesini, and M. K. Kim, "Quantitative phase-contrast confocal microscope," *Opt. Express*, vol. 22, no. 15, pp. 17830–17839, Jul. 2014.
- [71] N. Siegel and G. Brooker, "Improved axial resolution of FINCH fluorescence microscopy when combined with spinning disk confocal microscopy," *Opt. Express*, vol. 22, no. 19, pp. 22298–22307, Sep. 2014.
- [72] R. Kelner and J. Rosen, "Spatially incoherent single channel digital Fourier holography," *Opt. Lett.*, vol. 37, no. 17, pp. 3723–3725, Sep. 2012.
- [73] R. Kelner, J. Rosen, and G. Brooker, "Enhanced resolution in Fourier incoherent single channel holography (FISCH) with reduced optical path difference," *Opt. Express*, vol. 21, no. 17, pp. 20131–20144, Aug. 2013.
- [74] D. N. Naik, G. Pedrini, and W. Osten, "Recording of incoherent-object hologram as complex spatial coherence function using Sagnac radial shearing interferometer and a Pockels cell," *Opt. Express*, vol. 21, no. 4, pp. 3990–3995, Feb. 2013.
- [75] Y. Wan, T. Man, and D. Wang, "Incoherent off-axis Fourier triangular color holography," *Opt. Express*, vol. 22, no. 7, pp. 8565–8573, Apr. 2014.
- [76] T. Man, Y. Wan, F. Wu, and D. Wang, "Four-dimensional tracking of spatially incoherent illuminated samples using self-interference digital holography," *Opt. Commun.*, vol. 355, pp. 109–113, Jun. 2015.
- [77] K. Watanabe and T. Nomura, "Recording spatially incoherent Fourier hologram using dual channel rotational shearing interferometer," *Appl. Opt.*, vol. 54, no. 1, pp. A18–A22, Jan. 2015.
- [78] R. Kelner and J. Rosen, "Three-dimensional imaging by self-reference digital holograms," in *Proc. IEEE Int. Conf. Ind. Informat. (INDIN'15)*, Jul. 22–24, 2015.



Joseph Rosen received the B.Sc., M.Sc., and D.Sc. degrees in electrical engineering from the Technion-Israel Institute of Technology, Haifa, Israel, in 1984, 1987, and 1992, respectively.

He is a Benjamin H. Swig Professor of Optoelectronics with the Department of Electrical and Computer Engineering, Ben-Gurion University of the Negev, Beer-Sheva, Israel. He has co-authored about 200 scientific journal papers, book chapters, and conference publications. His research interests include digital holography, optical microscopy, diffractive optics, statistical optics, biomedical optics, optical computing, and image processing.

Dr. Rosen is a Fellow of the Optical Society of America (OSA) and the International Society for Optical Engineering (SPIE).



Roy Kelner received the B.Sc. (*magna cum laude*), M.Sc. (*magna cum laude*), and Ph.D. degrees in electrical and computer engineering from the Ben-Gurion University of the Negev, Beer-Sheva, Israel, in 2008, 2010, and 2015, respectively.

Currently, he is a Postdoctoral Fellow with the Department of Electrical and Computer Engineering, Ben-Gurion University of the Negev.